Rheology and Microscopic Topology of Entangled Polymeric Liquids

Ralf Everaers, *et al.*

Science **303**, 823 (2004);
DOI: 10.1126/science.1091215

Science (print ISSN 0036-8075; online ISSN 1095-9203) is published weekly, except the last week in December, by the American Association for the Advancement of Science, 1200 New York Avenue NW, Washington, DC 20005.

their aspect ratio and magnetic properties. This is not the case for iron because, whatever the ligands used, nanocubes of ~7 nm form. Furthermore, the interparticle distance in these samples is uniform and very short (1.6 nm), which tends to suggest the absence of coordinated long-chain ligands at the surface of the particles. This can result from the formation in all cases of hexamethyldisilazane, which can remain coordinated at the surface of the particles. It is also noteworthy that neither water formed upon condensation of OA with HDA in the reaction conditions nor chloride ions present in HDAC are detrimental to the formation and magnetic properties of the iron nanocubes.

References and Notes

1. S. Sun, C. B. Murray, D. Weller, L. Folks, A. Moser, *Science* **287**, 1989 (2000).
2. J. C. Mallinson, *Magneto-Resistive Heads: Fundamental and Applications* (Academic Press, New York, 1996).
3. R. P. Andres *et al.*, *Science* **272**, 1323 (1996).
4. C. T. Black, C. B. Murray, R. L. Sandstrom, S. Sun, *Science* **290**, 1131 (2000).
5. M. Respaud *et al.*, *Phys. Rev. B* **57**, 2925 (1998).
6. F. Dumestre *et al.*, *Angew. Chem. Int. Ed. Engl.* **41**, 4286 (2002).
7. N. Cordente *et al.*, *Nano Lett.* **1**, 565 (2001).
8. F. Dumestre *et al.*, *Angew. Chem. Int. Ed. Engl.* **42**, 5213 (2003).
9. K. S. Suslick, M. Fang, T. Hyeon, *J. Am. Chem. Soc.* **118**, 11960 (1996).
10. S. J. Park *et al.*, *J. Am. Chem. Soc.* **122**, 8581 (2000).
11. M. W. Grinstaff, M. B. Salamon, K. S. Suslick, *Phys. Rev. B* **48**, 269 (1993).
12. D. Farrell, S. A. Majetich, J. P. Wilcoxon, *J. Phys. Chem. B* **107**, 11022 (2003).
13. C. Nayral *et al.*, *Chem. Eur. J.* **6**, 4082 (2000).
14. K. Soulantica, A. Maisonnat, M. C. Fromen, M. J. Casanove, B. Chaudret, *Angew. Chem. Int. Ed. Engl.* **42**, 1945 (2003).
15. R. A. Andersen *et al.*, *Inorg. Chem.* **27**, 1782 (1988).
16. C. B. Murray *et al.*, *IBM J. Res. Dev.* **45**, 47 (2001).
17. V. F. Puntes, D. Zanchet, C. K. Erdonmez, A. P. Alivisatos, *J. Am. Chem. Soc.* **124**, 12874 (2002).
18. Z. A. Peng, X. Peng, *J. Am. Chem. Soc.* **123**, 1389 (2001).
19. V. F. Puntes, K. M. Krishnan, A. P. Alivisatos, *Science* **291**, 2115 (2001).
20. H. K. Lee *et al.*, *J. Appl. Phys.* **93**, 7047 (2003).
21. A. S. Edelstein, G. M. Chow, E. I. Altman, R. J. Colton, D. M. Hwang, *Science* **251**, 1590 (1991).
22. C. B. Murray, K. L. Stokes, K.-S. Cho, Abstracts of Papers, 225th American Chemical Society National Meeting, New Orleans, LA, 23 to 27 March 2003 (2003).

23. The authors thank CNRS and Motorola S.P.S. for support, V. Collière, L. Datas, and TEMSCAN service (Université Paul Sabatier Toulouse) for TEM, I. Fourquaux and B. Payré (Centre de Microscopie Electronique Appliquée à la Biologie. Université Paul Sabatier Toulouse) for ultramicrotomy, T. Aigouy (Laboratoire de Mecanismes de Transfert en Geologie, Université Paul Sabatier Toulouse) for x-ray diffraction, and R. Andersen (University of California, Berkeley), M. Respaud (Laboratoire de Nanophysique, Magnetisme et Optoelectronique Toulouse), and K. Soulantica (LCC Toulouse) for fruitful discussions.

Supporting Online Material

www.sciencemag.org/cgi/content/full/303/5659/821/DC1
Figs. S1 to S5

16 October 2003; accepted 22 December 2003

Rheology and Microscopic Topology of Entangled Polymeric Liquids

Ralf Everaers,[1,2]* Sathish K. Sukumaran,[1] Gary S. Grest,[3] Carsten Svaneborg,[1] Arvind Sivasubramanian,[1] Kurt Kremer[1]

The viscoelastic properties of high molecular weight polymeric liquids are dominated by topological constraints on a molecular scale. In a manner similar to that of entangled ropes, polymer chains can slide past but not through each other. Tube models of polymer dynamics and rheology are based on the idea that entanglements confine a chain to small fluctuations around a primitive path that follows the coarse-grained chain contour. Here we provide a microscopic foundation for these highly successful phenomenological models. We analyze the topological state of polymeric liquids in terms of primitive paths and obtain parameter-free, quantitative predictions for the plateau modulus, which agree with experiment for all major classes of synthetic polymers.

The relation between the complex viscoelastic properties of polymer liquids and their microscopic structure and dynamics is a key issue in modern materials science and biophysics (*1*–*3*). A prototypical example is natural rubber. Strictly speaking, natural rubber is a (highly viscous) liquid, even though over a large frequency range it presents the same rubber-elastic response to oscillatory mechanical deformations as vulcanized rubber (*4*). This response can be characterized by a temperature- and concentration-dependent material constant, the plateau shear modulus G_N^0, which is on the order of 10^6 Pa, or five orders of magnitude smaller than the shear modulus of ordinary solids. The origin of this behavior can be traced back to the molecular scale. Natural rubber consists of linear chain molecules of up to $N \approx 3 \times 10^4$ monomer units with molecular masses up to $M = 10^6$ g/mol and contour lengths up to $L = 10$ μm. Individual polymers adopt random coil conformations. The coil diameter of about 100 nm is much smaller than the chain contour length, but substantially larger than the diameter of the corresponding densely packed globule of ~20 nm. Consequently, neighboring chains strongly interpenetrate and entangle with each other. In our example, a spherical volume with the coil diameter contains about 150 polymers. Although the chain length has essentially no effect on the magnitude of G_N^0, it strongly influences the time or frequency interval for which the plateau in the shear relaxation modulus $G_N(\omega)$ can be observed (*1*). For natural rubber (*5*, *6*), one can estimate that the relaxation-time increases from $\tau_d(M = 10^4$ g/mol$) \approx 5 \times 10^{-5}$ s to $\tau_d(M = 10^6$ g/mol$) \approx 5$ s and would reach years for chains with molecular masses of 10^8 g/mol even though their typical spatial extension is only on the order of 1 μm.

All melts or semidilute solutions of sufficiently long flexible chain molecules show the same, universal behavior (*1*). Early theories treated entanglements as transient physical cross-links to capture the analogy to rubber-elastic polymer networks. Modern theories of polymer dynamics are based on the idea that Brownian motion is dominated by the restriction that the chains may slide past but not through each other. Consequently, the motion of each polymer chain is thought to be confined to a tubelike region around a so-called primitive path along the coarse-grained chain contour (*7*) (Fig. 1). The stress relaxation is effectively suspended up to the time $\tau_d(N)$ required by the chains to leave or renew their deformed original tubes. The basic version of the tube model considers only a single relaxation mechanism: one-dimensional, curvilinear diffusion in tubes of fixed length ("reptation") (*8*). Its prediction $\tau_d(N) \propto N^3$ agrees with experimental data in the limit of large N (*9*). Convincing microscopic evidence for both tube confinement and reptation dynamics has been accumulated from experiments and computer simulations (*10*–*12*). Recent, more refined analytical (*2*) and numerical models (*13*–*17*) of the dynamics of the primitive paths account for additional relaxation mechanisms and quantitatively describe most rheological and single-chain

[1]Max-Planck-Institut für Polymerforschung, Ackermannweg 10, 55128 Mainz, Germany. [2]Max-Planck-Institut für Physik komplexer Systeme, Nöthnitzer Str. 38, 01187 Dresden, Germany. [3]Sandia National Laboratories, Albuquerque, NM 87185, USA.

*To whom correspondence should be addressed. E-mail: everaers@mpipks-dresden.mpg.de

dynamics data with a small set of physically motivated, material-specific parameters such as the tube diameter, d_T.

What is still lacking, however, is an understanding of the microscopic foundations of the tube model. Entanglements impose topological constraints on polymer conformations (*18*) similar to those one experiences in manipulating a knotted string. However, so far theoretical (*18*, *19*) and computational (*20*, *21*) efforts to introduce elements from mathematical knot theory into polymer statistical mechanics (Fig. 1C) have not led to a systematic derivation of the tube model or its parameters. Here we follow the opposite strategy and introduce a physically motivated analysis of the melt topology in terms of primitive paths (Fig. 1B). The idea is to simultaneously establish the microscopic foundations of the tube model and to endow a highly successful phenomenological model with predictive power for structure-property relations. In the present, first step, we concentrate on the plateau modulus and the origin of its experimentally observed dependence on the melt structure.

The static structure of polymer melts and good-solvent semidilute solutions can be discussed in terms of two length scales: the Kuhn length, l_K (*1*), and the packing length, p (*22*). Both characteristic scales depend in a nontrivial way on the microscopic interactions, temperature, pressure, concentration, etc., and can usually neither be varied directly nor independently in experiments or simulations. The Kuhn length characterizes the conformations of individual chains and is defined as the step length of a random walk with the same contour length, L, and mean-square end-to-end distance $\langle R^2\rangle = l_K L$ as those of the actual chains. Although locally most monomers belong to the same chain, random coils are strongly interpenetrating on large scales. The packing length, $p = [\rho_{chain}\langle R^2\rangle]^{-1}$, is the characteristic length scale at which polymers start to interpenetrate. (The product of the number density of chains, ρ_{chain}, and of $\langle R^2\rangle$ is independent of chain length for a fixed monomer number density, ρ.) Plateau moduli can be compared by plotting dimensionless numbers such as $G_N^0 l_K^3/k_BT$ as a function of the ratio l_K/p (*22*). The experimental data for dense melts shown in Fig. 2 result from a substantial effort made in recent years (*23*–*25*) to synthesize monodisperse high molecular weight samples for a wide range of different polymer species. These samples were carefully characterized by rheological measurements, and in many cases the microscopic chain structure was determined in small-angle neutron-scattering experiments. The accessible l_K/p range can be extended appreciably by including data for entangled semidilute solutions of polymers in good solvents (*26*–*28*). All data points follow the empirical relation $G_N^0 = 0.00226 k_BT/p^3$ (*24*), which implies a simple proportionality $d_T \propto p$ between tube diameter and packing length.

In order to study generic properties of entangled polymers in computer simulations, it is not necessary to resort to atomistic simulations of a specific chemical species. Rather, one can choose a coarse-grained model that combines numerical efficiency with the characteristic features of (synthetic) polymers: connectivity, flexibility, local liquid-like monomer packing, and mutual uncrossability of the chain backbones. Here, we mainly investigate dense melts and semidilute solutions of bead-spring polymers with variable intrinsic stiffness. Chain segments are represented as spheres with short-ranged excluded volume interactions. Model polymers are formed by connecting beads via springs. The parameter choice guarantees a sufficiently close contact between connected monomers to prevent chain crossings (*29*–*32*). In addition, we present results for a coarse-grained model for polycarbonate (BPA-PC) (*33*, *34*). In all cases, the characteristic lengths l_K and p are determined directly from the polymer conformations in equilibrated melt or solution samples. In some cases, we have determined the plateau moduli in extensive simulations of strained melts (*35*–*37*) (Table 1). The good agreement with the experimental data in Fig. 2 confirms the insensitivity of entanglement effects to atomistic details. Furthermore, it provides the necessary validation of our generic bead-spring models as well as the systematically coarse-grained polycarbonate model, and establishes direct simulation as a (rather expensive) brute-force approach for studying rheological structure-property relations.

The key idea in this report is the analysis of the topology of entangled melts on

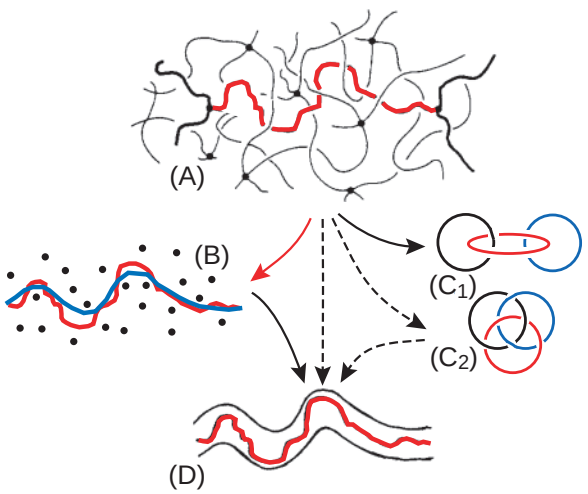

Fig. 1. Relation between different theoretical approaches to describe entanglement effects in polymeric liquids. (**A**) Schematic view of an entangled and cross-linked polymer melt. The thermal fluctuations of the red strand are reduced due to a caging effect from nearby chains. (**B**) The primitive path (blue) corresponding to the red chain conformation in an array of fixed obstacles is the shortest connection between the chain ends that can be reached from the initial conformation without crossing any obstacles. The relation between the primitive path (B) and the tube (D) description is straightforward. (**C**) Topological theories propose to specify entanglements in terms of an (infinite) series of topological invariants for pairs (C_1), triplets (C_2), etc., of closed loops and to integrate the conservation of these invariants under strain into the statistical mechanical analysis (*18*–*21*). Unfortunately, it is diffcult to progress beyond the pair term (C_1), and so far no systematic derivation of the tube model along these lines exists. (**D**) Tube model. In a single-chain picture, entanglements are represented by an effective potential. The challenge is to predict the parameters of the tube model from the molecular structure. Our primitive-path analysis allows us to systematically derive the parameters of the tube model by passing from (A) over (B) to (D).

Table 1. System characteristics and results from the primitive-path analysis for bead-spring chain melts (I to IV) and semidilute solutions (V and VI), as well a coarse-grained model for a polycarbonate melt (BPA-PC). The N_e values quoted for BPA-PC refer to chemical repeat units.

		Melts					Solutions	
		I	II	III	IV	BPA-PC	V	VI
Structure	ρ/σ^3	0.85	0.85	0.85	0.85	0.85	0.134	0.231
	l_K/σ	1.82	2.16	2.79	3.34	4.36	2.98	2.85
	p/σ	0.68	0.56	0.43	0.36	0.37	2.28	1.38
Rheological simulations	$10^3 G_N^0\sigma^3/k_BT$	9.7 ± 1.4	–	23 ± 3	–	34 ± 14	–	–
	N_e	70 ± 10	–	30 ± 4	–	5 ± 2	–	–
Primitive path analysis	a_{pp}/σ	10.7 ± 0.5	9.7 ± 0.3	8.7 ± 0.1	8.6 ± 0.2	8.9 ± 0.7	34.5 ± 0.3	24.3 ± 3.4
	N_e	65 ± 7	45 ± 3	28 ± 1	23 ± 1	6 ± 1	363 ± 6	188 ± 52

the basis of the concept of primitive paths introduced by Edwards (*38*) to complement his tube model (*7*). Edwards considered a test chain embedded in an array of rigid, infinitely thin, spatially fixed line obstacles representing the constraints imposed by the other polymers on thermal fluctuations of the test chain (Fig. 1B). He identified the random walk–like axis of the tube with what the called the "primitive" path: the shortest path between the endpoints of the original chain into which its contour can be contracted without crossing any obstacle. Similar to the tube, the primitive path is usually discussed without specifying the relation between the obstacles and the melt structure. Here we argue that the obstacles encountered by a test chain are themselves polymers with identical properties and propose to apply the primitive-path analysis to all polymers in the system simultaneously.

The implementation of this idea into a simulation code for bead-spring chains is straightforward: First, the chain ends are fixed in space. Then, the intrachain excluded-volume interactions are disabled, while retaining the interchain excluded-volume interactions. Finally the energy of the system is minimized by slowly cooling the system toward $T = 0$ (*39*). Without thermal fluctuations and intrachain excluded-volume interactions, the bond springs try to reduce the bond length to zero and pull the chains taut. The interchain excluded-volume interactions ensure that different chains do not cut through each other, and thus the topology is conserved throughout the procedure. The result of such an analysis is a mesh of primitive paths (Fig. 3). The primitive-path analysis automatically accounts for multichain entanglements of arbitrary order (Fig. $1C_2$).

Figure 3 shows that individual primitive paths consist of straight segments of strongly fluctuating length and more or less sharp turns at entanglement points between two paths. Being random walks, they can be characterized by a Kuhn length, a_{pp}, and a contour length, L_{pp}. Compared to the original chains, the line tension leads to a reduction of the contour length $L_{pp} \ll L$. Due to the fixed endpoint positions $\langle R^2_{pp} \rangle \equiv \langle R^2 \rangle$, it follows that $L_{pp} a_{pp} \equiv L l_K$. Thus, the primitive paths must have a correspondingly larger Kuhn length in order to reach the same spatial extension as the original chains (*1*). Figure 4 illustrates this point by showing a comparison of the mean-square spatial distances $\langle r^2 | i - j | \rangle$ and $\langle r^2_{pp} | i - j | \rangle$ between pairs of monomers i and j for the original chains and the primitive paths, respectively. It is sufficient to extract a single number, the average bond length of the primitive paths, b_{pp}, to determine $L_{pp} = N b_{pp}$, $a_{pp} = \langle R^2 \rangle / L_{pp}$ as well as $\langle r^2_{pp} | i - j | \rangle$ for arbitrary chemical distances $|i - j|$ (Fig. 4). For all systems studied, $L_{pp} \ll a_{pp}$, i.e., our chains are sufficiently long to be multiply entangled. In this limit, the primitive paths reach essentially the same overall extension as the original chains for chemical distances $|i - j| \ll N$, so that we can neglect finite-N effects in our analysis.

An intuitive way to characterize the topological state of (bead-spring) melts and solutions is to calculate the number of monomers between entanglements (often referred to as entanglement "length"), which is given by the number of monomers per Kuhn segment of the primitive path, $N_e = a_{pp}/b_{pp}$. Our results are summarized in Table 1. For the bead-spring systems, the extracted values for the entanglement lengths vary over a wide range $23 \leq N_e \leq 363$, and we find that (i) stiff chains are more strongly entangled than flexible chains and (ii) dilution reduces the number of entanglements. In the case of polycarbonate, we properly reproduce the extraordinarily short entanglement length of $N_e \simeq 6$ monomers reported in the literature (*22*).

Having supplied a microscopic definition of primitive paths as physical observables and having determined their properties for melt and solution configurations of entangled bead-spring model polymers, we are now in a position to test the predictive power of the tube model. For this purpose, we use the standard expression (*1*)

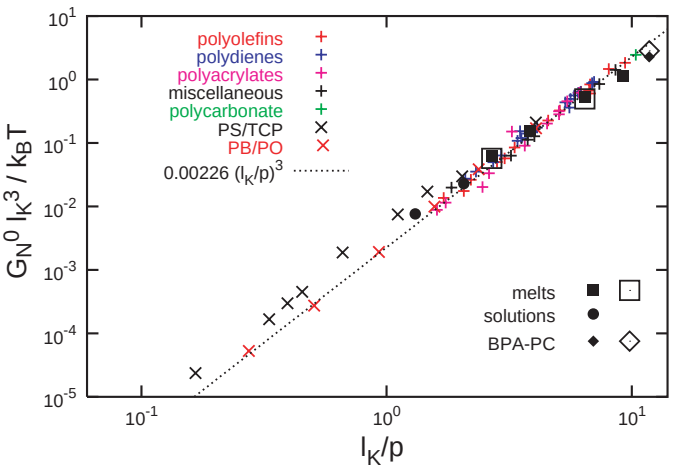

Fig. 2. Dimensionless plateau moduli $G l_K^3 / k_B T$ as a function of the dimensionless ratio l_K/p of Kuhn length l_K and packing length p. The figure contains (i) experimentally measured plateau moduli for polymer melts (*25*) (+; colors mark different groups of polymers as indicated) and semidilute solutions (*26–28*) (×); (ii) plateau moduli inferred from the normal tensions measured in computer simulation of bead-spring melts (*35*, *36*) (□) and a semi-atomistic polycarbonate melt (*37*) (◇) under an elongational strain; and (iii) predictions of the tube model Eq. 1 based on the results of our primitive-path analysis for bead-spring melts (■), bead-spring semidilute solutions (●), and the semi-atomistic polycarbonate melt (◆). The line indicates the best fit to the experimental data for polymer melts by Fetters *et al.* (*24*). Errors for all the simulation data are smaller than the symbol size.

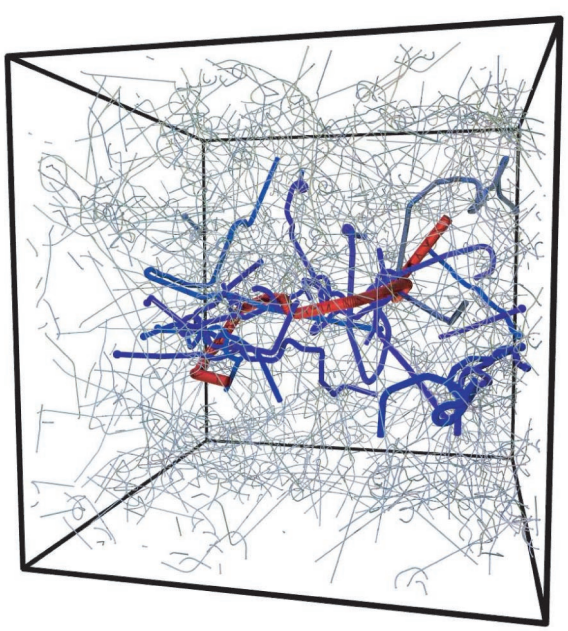

Fig. 3. Result of the primitive-path analysis of a melt of 200 chains of $N + 1 = 350$ beads. We show the primitive path of one chain (red) together with all of those it is entangled with (blue). The primitive paths of all other chains in the system are shown as thin lines.

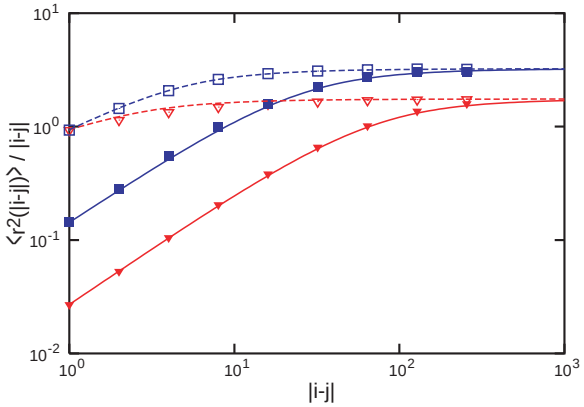

Fig. 4. Mean-square monomer distances for the original chain conformations (open symbols) and for the primitive paths (filled symbols) as a function of chemical distance. Results are shown for two sets of equilibrated melts of bead-spring polymers with persistence length $l_K = 1.82\sigma$ (▽) and $l_K = 3.34\sigma$ (□). The lines represent a well-known theoretical expression (*30*) for freely jointed chains with the same contour length and asymptotic mean-square end-to-end distance as those of our bead-spring chains and primitive paths, respectively.

$$G_N^0 = \frac{4}{5}(k_BT/pa_{pp}^2) = \frac{4}{5}(\rho k_BT/N_e) \quad (1)$$

which relates the plateau modulus to the Kuhn length of the primitive path. The results are listed in Table 1, and we note excellent agreement in those cases for which we also determined the plateau modulus in simulations of stretched melts. Moreover, the comparison to the available experimental data in Fig. 2 suggests that our topological analysis enables the tube model to predict plateau moduli from first principles.

The primitive-path analysis also provides insight into the apparent proportionality of p and d_T (*24*). So far, we have characterized the statistics of individual primitive paths in terms of their Kuhn length, a_{pp}. However, if we think of the limitation of transverse fluctuations of a polymer around its primitive path as being due to a cage formed by the surrounding paths, then it makes sense to take a closer look at the mesh size, $\xi_{pp} \equiv (\rho_{chain}L_{pp})^{-1/2}$, of the primitive path mesh shown in Fig. 3. From the definition of the packing length, $p \equiv [\rho_{chain}\langle R^2\rangle]^{-1}$, and the identity $\langle R^2\rangle = L_{pp}a_{pp}$, one immediately obtains the relation

$$pa_{pp} \equiv \xi_{pp}^2 \quad (2)$$

which shows that ξ_{pp} can have a different dependence on l_K and p than a_{pp}.

In contrast to semidilute solutions in θ solvents (*27*), there is no evidence for a second, independent length scale characterizing entanglements in dense melts of intrinsically flexible polymers. In this case, Eq. 2 directly implies the experimentally observed relation $d_T \propto a_{pp} \propto \xi_{pp} \propto p$, shedding new light on the physics underlying the packing argument as well as on the implications of competing proposals [for references, see (*40*)]. Finally, Eq. 1 is only valid for $l_K \ll a_{pp}$, i.e., if the chains inside the tube can be considered as entropic springs. The parameters of our stiffest bead-spring chains and of the polycarbonate model are already close to the crossover to a different regime, where the elastic response is caused by bending of tightly entangled semiflexible chains (*41*).

To summarize, we have introduced a microscopic definition of the key quantity of most current theories of polymer dynamics and rheology (*1*, *2*): the primitive paths characterizing the topological state of an entangled polymeric liquid. In the present first step, we have concentrated on their static properties. The comparison to a wide range of experimental data suggests that the tube model can make parameter-free, quantitative predictions for plateau moduli on the basis of our purely topological analysis. This paves the way to a systematic investigation of the dynamic processes described by the tube model and of the relation between its parameters and the microscopic structure of the polymeric liquids.

References and Notes

1. M. Doi, S. F. Edwards, *The Theory of Polymer Dynamics* (Clarendon, Oxford, 1986).
2. T. C. B. McLeish, *Adv. Phys.* **5**, 1379 1527 (2002).
3. D. Boal, *Mechanics of the Cell* (Cambridge Univ. Press, Cambridge, 2002).
4. L. R. G. Treloar, *The Physics of Rubber Elasticity* (Clarendon, Oxford, 1975).
5. Y. Matsumiya, H. Watanabe, T. Inoue, K. Osaki, M. L. Yao, *Macromolecules* **31**, 7973 (1998).
6. D. W. van Krevelen, *Properties of Polymers* (Elsevier, Amsterdam, 1990).
7. S. F. Edwards, *Proc. Phys. Soc.* **92**, 9 (1967).
8. P. G. de Gennes, *J. Chem. Phys.* **55**, 572 (1971).
9. R. Colby, L. J. Fetters, W. W. Graessley, *Macromolecules* **20**, 2226 (1987).
10. K. Kremer, G. Grest, *J. Chem. Phys.* **92**, 5057 (1990).
11. P. Schleger, B. Farago, C. Lartigue, A. Kollmar, D. Richter, *Phys. Rev. Lett.* **81**, 124 (1998).
12. J. Käs, H. Strey, E. Sackmann, *Nature* **368**, 226 (1994).
13. Y. Masubuchi *et al.*, *J. Chem. Phys.* **115**, 4387 (2001).
14. J. T. Padding, W. J. Briels, *J. Chem. Phys.* **117**, 925 (2002).
15. K. Iwata, M. Tanaka, N. Mita, Y. Kohno, *Polymer* **43**, 6595 (2002).
16. M. Doi, J. Takimoto, *Philos. Trans. R. Soc. London Ser. A* **361**, 641 (2003).
17. J. D. Schieber, J. Neergaard, S. Gupta, *J. Rheol.* **47**, 213 (2003).
18. S. F. Edwards *Proc. Phys. Soc.* **91**, 513 (1967).
19. K. Iwata, S. F. Edwards, *J. Chem. Phys.* **90**, 4567 (1989).
20. R. Everaers, K. Kremer, *Phys. Rev. E* **53**, R37 (1996).
21. W. Michalke, M. Lang, S. Kreitmeier, D. Göritz, *Phys. Rev. E* **64**, 012801 (2001).
22. W. W. Graessley, S. F. Edwards, *Polymer* **22**, 1329 (1981).
23. L. J. Fetters, D. J. Lohse, D. Richter, T. A. Witten, A. Zirkel, *Macromolecules* **27**, 4639 (1994).
24. L. J. Fetters, D. J. Lohse, W. W. Graessley, *J. Polym. Sci. B Polym. Phys.* **37**, 1023 (1999).
25. L. J. Fetters, D. J. Lohse, S. T. Milner, W. W. Graessley, *Macromolecules* **32**, 6847 (1999).
26. R. Colby, L. J. Fetters, W. G. Funk, W. W. Graessley, *Macromolecules* **24**, 3783 (1991).
27. T. Inoue, Y. Yamashita, K. Osaki, *Macromolecules* **35**, 9169 (2002).
28. Note, however, that for the solutions $\langle R^2\rangle$ was not determined independently by small-angle neutron scattering. Hence, we used standard scaling relations to estimate the chain dimensions.
29. Monomers are modeled as spheres of diameter σ interacting through a truncated 6-12 Lennard-Jones potential, which is short-ranged and purely repulsive. The polymers are formed by connecting beads via springs. The average bond length is $b = 0.97\sigma$. The parameter choice ensures that two chains cannot cross each other in dynamic simulations. We have studied monodisperse polymer melts of $M = 80$ to 500 chains of length $50 \le N \le 700$ at a bead density of $\rho = 0.85\sigma^{-3}$. By introducing a small intrinsic bond bending potential, l_K is varied between 1.82σ and 3.34σ. For details, see (*30*).
30. R. Auhl, R. Everaers, G. S. Grest, K. Kremer, S. J. Plimpton, *J. Chem. Phys.* **119**, 12718 (2003).
31. For semidilute and dense solutions, we only studied fully flexible chains swollen in an athermal (vacuum) solvent. Each solution consists of $M = 50$ chains of length $N = 1000$. The conformations were provided by B. Dünweg and P. Ahlrichs (*32*).
32. P. Ahlrichs, R. Everaers, B. Dünweg, *Phys. Rev. E* **64**, 040501 (2001).
33. For the BPA-PC model (*34*), we analyzed melt configurations for $M = 100$ chains of $N = 60$ chemical repeat units, which are represented by four beads each.
34. C. F. Abrams, K. Kremer, *Macromolecules* **36**, 260 (2003).
35. M. Pütz, K. Kremer, G. S. Grest, *Europhys. Lett.* **49**, 735 (2000).
36. M. Pütz, K. Kremer, unpublished data.
37. S. Leon, K. Kremer, in preparation.
38. S. F. Edwards, *Br. Polym. J.* **9**, 140 (1977).
39. For the harmonic bond potential used, the ground state is, apart from end effects, well defined. Topology conservation is ensured throughout the procedure, because the energy barrier for chain crossing increases for decreasing bond lengths, while thermal fluctuations are suppressed as the system is cooled. The detailed form of the excluded-volume potential affects the results only through the small diameter of the primitive paths, causing a slight increase of b_{pp} relative to the ideal case of infinitely thin entangled lines. The present algorithm disregards intrachain entanglements. As studies on ring polymers show, they are only of minor relevance. We are currently working on a variant of the algorithm that overcomes these limitations.
40. R. H. Colby, M. Rubinstein, J. L. Viovy, *Macromolecules* **25**, 996 (1992).
41. D. C. Morse, *Phys. Rev. E* **63**, 031502 (2001).

42. R.E. gratefully acknowledges financial support from an Emmy-Noether-Fellowship of the Deutsche Forschungsgemeinschaft and the hospitality of the Institute for Theoretical Physics at the University of California, Santa Barbara. S.K.S. is grateful to V. Lobaskin for help with some simulation data. A.S. was supported through the International Max Planck Research School for Polymer Materials Science, Mainz. Sandia is a multiprogram laboratory operated by Sandia Corporation, a Lockheed Martin Company, for the U.S. Department of Energy's National Nuclear Security Administration under contract DEAC04-94AL85000.

8 September 2003; accepted 6 January 2004